University of Zawia Journal of Engineering Sciences and Technology (UZJEST)
Volume 4, Issue 2, (2026), pp 96-112, ISSN 3006-2764

Missile Aerodynamics Optimization Using Genetic Algorithm

Abdurrazag Khaled [*1], Hiba Almosrati [1], Jawaher Alkiza [*1]

[1] Aeronautical Engineering Department, Faculty of Engineering, University of Zawia, Zawia, Libya,

Corresponding author email: abkfx84@gmail.com

Received: 09-08-2026 | Accepted: 30-08-2026 | Available online: 09-09-2026 | DOI: 10.26629/uzjest.2026.08

ABSTRACT

This study presents a numerical optimization framework that integrates a Genetic Algorithm (GA) with the Missile Aerodynamic Prediction Program (MAPP) to enhance the aerodynamic performance of wing-body configurations at supersonic speeds. MAPP, based on United States Air Force (USAF) DATCOM methods, predicts longitudinal aerodynamic coefficients, including lift and drag. The GA shell was coupled with MAPP via a FORTRAN subroutine to maximize the lift-to-drag ratio (L/D) for wing-alone, body-alone, and wing-body configurations under geometric constraints. Validation against experimental data at Mach 1.99 showed excellent agreement. Optimization results showed clear improvements for all configurations. Wings performed better, bodies improved the most at certain Mach numbers, and wing-body combinations also showed strong gains. This integrated GA-MAPP tool offers an efficient, reliable method for supersonic aerodynamic shape optimization, with strong potential for application in advanced aircraft design.

Keywords: Supersonic Aerodynamics; Genetic Algorithm; Wing-Body Optimization; Lift-to-Drag Ratio; DATCOM; MAPP Program.

تحسين الديناميكية الهوائية للصواريخ باستخدام الخوارزمية الجينية

عبدالرزاق خالد[1]، هبة المصراتي[1]، جواهر الكيزة[1*]

[1]قسم هندسة الطيران، كلية الهندسة الزاوية، جامعة الزاوية، الزاوية، ليبيا

ملخـــــــص البحـــــــث

تقدم هذه الدراسة إطاراً عددياً للتّحسين يدمج الخوارزمية الجينية (GA) مع برنامج توقّع الديناميكا الهوائية للصواريخ (MAPP) بهدف تعزيز الأداء الديناميكي الهوائي لتشكيلات جسم مع جناح عند سرعات تفوق سرعة الصوت. يعتمد برنامج MAPP على طرق (USAF DATCOM) في توقّع المعاملات الديناميكية الهوائية ، والتي تشمل قوتي الرفع والأعاقة. وقد تم ربط الإطار الجيني ببرنامج MAPP عبر دالة فرعية مكتوبة بلغة FORTRAN لزيادة نسبة الرفع الى الأعاقة (L/D) لتشكيلات الجناح فقط ، والجسم فقط ، والجسم مع الجناح، في ظل قيود هندسية. أظهرت عمليات التحقق من النتائج، بمقارنتها مع البيانات التجريبية عند عدد ماخ 1.99، تطابقاً ممتازاً. كما كشفت نتائج التحسين عن تحسينات أداء كبيرة. قد أدّت الأجنحة أداءً أفضل، بينما شهدت الأجسام التحسّن الأكبر عند أعداد ماخ معينة، كما حققت تشكيلات الجناح والجسم مكاسب قوية أيضًا. تقدّم هذه الأداة

المتكاملة (GA–MAPP) طريقة فعّالة وموثوقة لتحسين الشكل الديناميكي الهوائي عند السرعات فوق الصوتية، مع إمكانات تطبيقية واعدة في تصميم الطائرات المتطورة.

الكلمات الدالة: الديناميكا الهوائية فوق الصوتية، الخوارزمية الجينية، تحسين تشكيلات الجسم مع الجناح، نسبة الرفع إلى الأعاقة، نظام DATCOM ، برنامج MAPP.

1. Introduction

Optimization has become essential across all major engineering disciplines, driven by the goal of producing economically viable products with embedded quality. Better design and production tools, along with low-cost computing, have enabled optimization methods, especially in aerospace engineering. Even without a physical product, optimization helps refine problems. The desire to make things better is a constant drive in engineering design [1].

Significant improvements in the calculation of lift and drag have transformed modern aerodynamics using genetic algorithms. In the past, engineers relied heavily on wind tunnel testing and simplified theoretical models, which were time-consuming and often inaccurate for complex shapes [2]. By applying genetic algorithms, search techniques inspired by natural selection, designers can now automatically explore thousands of possible airfoil or wing shapes, testing combinations of parameters to gradually evolve better solutions [1]. Aerodynamic geometry plays an important role in determining flow behavior and aerodynamic performance. Surface modifications can enhance aerodynamic characteristics [3], while numerical studies of complex airfoil configurations provide insights into turbulent flow behavior [4]. Compressible-flow simulations and advanced numerical methods are also essential for accurately predicting aerodynamic flow fields [5,6].

The application of genetic algorithms to missile aerodynamic shape optimization was pioneered by Anderson et al. [7], who demonstrated the capability of genetic algorithms to determine high-efficiency missile geometries for both single- and multiple-goal applications. For supersonic wing-body configurations, Sasaki and Obayashi [8] developed an automated aerodynamic optimization system using multiobjective evolutionary algorithms. The approach simultaneously optimized the wing and body to reduce aerodynamic drag. Oyama, Obayashi, and Nakahashi [9] applied evolutionary algorithms to the Euler/Navier-Stokes optimization of supersonic wing designs.

More recently, a multiobjective genetic algorithm was applied to missile aerodynamic shape optimization, achieving significant improvements in lift-to-drag ratio across various Mach numbers, demonstrating the effectiveness of GA-based methods for missile aerodynamic optimization. Liu and Chen [10] applied genetic algorithms with gradient-based local search to supersonic wing planform optimization, demonstrating improved convergence characteristics. Michelotti et al. [11] implemented genetic algorithms for supersonic airfoil optimization, further validating the effectiveness of GA-based approaches for aerodynamic shape design.

The Missile Aerodynamic Prediction Program (MAPP) serves as the foundation for this study and is employed as a design tool developed for the preliminary estimation of longitudinal aerodynamic characteristics of wing, body, and wing-body configurations at supersonic speeds. MAPP is built upon the USAF Stability and Control DATCOM [12, 13], which refers to a comprehensive, systematic collection of engineering methods and data for predicting the stability and control characteristics of an aircraft.

Despite significant advances in computational aerodynamics, the design of efficient supersonic wing-body configurations remains challenging due to the complex, nonlinear interactions between geometric parameters and aerodynamic performance. This research addresses this challenge by developing an automated optimization framework that combines the global search capabilities of genetic algorithms with the empirically validated prediction methods of the MAPP.

For wing-body configurations, the key design variables include root chord, span, leading-edge sweep, trailing-edge sweep, body diameter, body length, nose shape, and position of the wing on the body [14]. During the optimization process, the aerodynamic prediction code MAPP is called many times in an iterative loop. Design parameters are constants that remain fixed when comparing different designs, including wing airfoil section, wing thickness, body cross-section, and nose type.

2. Methodology

2.1 Missile Aerodynamics Prediction Program

The MAPP is sufficient for sea-level conditions, for triangular or trapezoidal wing configurations, bodies with cylindrical mid-sections with conical or ogival noses, and for wing-body configurations.
Wing Parameters: Key geometric parameters include wing span (b), root chord (c_r), tip chord (c_t), taper ratio ($\lambda = c_t/c_r$), sweep angles of leading and trailing edges (Λ_{LE}, Λ_{TE}), and aspect ratio ($A = b^2/S$). The Mean Aerodynamic Chord (MAC) is calculated as:

$$\bar{c} = \frac{2}{3} c_r \left(\frac{1+\lambda+\lambda^2}{1+\lambda}\right) \tag{1}$$

2.2 Aerodynamics Prediction Methods

2.2.1 Wing Aerodynamics

Lift Prediction: For supersonic speeds, the Method of Characteristics (MOC) is more accurate than linear theory. Unlike linear theory's constant slope of $4/\sqrt{M^2-1}$, MOC accounts for real shocks/expansions, yielding a slope that varies with thickness, angle of attack, and Mach number often lower than linear predictions for thicker sections and higher alpha. Accurate wing lift data is critical, as many calculations depend on it. The assumptions made must be clearly understood.

At supersonic speeds, pressure forces act more perpendicular to the chord (normal force, $C_{N\alpha}$). For small alpha, $C_{L\alpha} \approx C_{N\alpha}$; at higher angles, the distinction matters [2]. Theory predicts $C_{N\alpha}$ well except where thickness effects are significant, primarily when Mach numbers are near the leading-edge condition. For sharp leading edges, the nose angle determines shock position and thus $C_{N\alpha}$. Corrections are applied using empirical factors for wings approaching sonic leading edges [15].

A generalized method calculates lift from 0° to 90° using

$$\frac{C_L}{\cos\alpha} = C_{N_\alpha} \frac{\sin 2\alpha}{2} + C_{N_{\alpha\alpha}} sin\alpha\,|sin\alpha| \tag{2}$$

where $C_{N\alpha}$ is the linear theory slope, and $CN_{\alpha\alpha}$ is an empirical nonlinear coefficient.

Supersonic Wing Lift Categories

Wings are categorized by leading edge (L.E.) condition:

Subsonic Leading Edges ($\beta/\tan(\Lambda_{L.E.}) \leq 1$): Nonlinearity depends on $\beta/\tan(\Lambda_{L.E.})$ and $C_{N\alpha}$. For sweeps <62.5°, use linear $C_{N\alpha}$; for >62.5°, apply an empirical correction.

Supersonic Leading Edges ($\beta/\tan(\Lambda_{L.E.}) > 1$): Shocks may be attached or detached. Shock detachment occurs when the normal angle of attack plus semiwedge angle exceeds a critical value,

$$\alpha_\perp + \delta_\perp > \frac{4}{3\sqrt{3}(\gamma+1)} \frac{(M_\perp^2-1)^{3/2}}{M_\perp^2} \tag{3}$$

For attached shocks, use shock expansion theory. For detached shocks, no exact theory exists; an empirical nonlinear coefficient is used.

Drag Prediction: Wing zero-lift drag comprises skin friction and pressure drag. Friction drag, dominant at subsonic speeds and significant supersonically, arises from boundary-layer shear. The flow may be laminar, turbulent, or mixed; fully turbulent flow is assumed for supersonic speeds. At supersonic speeds, pressure drag is primarily wave drag [12].

The supersonic zero-lift drag coefficient (based on Sref) is:

$$C_{D_0} = C_{D_f} + C_{D_w} \tag{4}$$

Where: Skin friction drag coefficient is obtained as:

$$C_{D_f} = C_f \frac{S_{wet}}{S_{ref}} \tag{5}$$

The wave drag coefficient follows linear supersonic theory, using an effective thickness ratio and basic planform. Distinction is made between sharp-nosed and round-nosed airfoils (In this research, the sharp-nosed airfoils are used) [12].

Sharp-nosed airfoils:

Supersonic leading edge ($\beta/\cot(\Lambda_{\text{L.E.}})_{\text{bw}} \geq 1$):

$$C_{D_w} = \frac{k}{\beta}\left(\frac{t}{c}\right)^2_{eff} \frac{S_{bw}}{S_{ref}} \tag{6}$$

Subsonic leading edge ($\beta/\cot(\Lambda_{\text{L.E.}})_{\text{bw}} < 1$):

$$C_{D_w} = k cot \Lambda_{\text{L.E}_{\text{bw}}} \left(\frac{t}{c}\right)^2_{eff} \frac{S_{bw}}{S_{ref}} \tag{7}$$

where *k* depends on the airfoil section, as given in Table 1.

Table 1. Illustrates a sharp-nosed airfoil.

Basic Wing Airfoil Section	k	Section
Biconvex	$\frac{16}{3}$	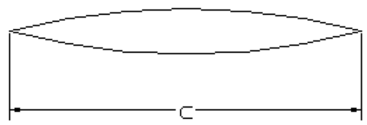
Double Wedge	$\frac{c\, x_t}{1 - {x_t}/{c}}$	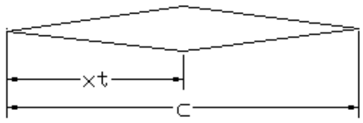
Hexagonal	$\frac{c\,(c - x_2)}{x_1\, x_3}$	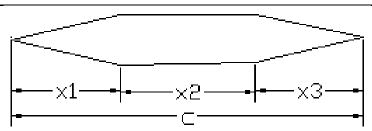

Total drag at angle of attack:

$$C_D = C_{D_0} + C_{D_L} \tag{8}$$

where C_{DL} is drag due to lift, approximately proportional to C_L^2:

$$C_{D_L} = \frac{K C_L^2}{\pi A} \tag{9}$$

Where *K* is the drag due to the lift factor. The C_{DL} can be written into two terms, the well-known induced drag C_{Di} and viscous drag due to lift C_{Dv}, so that

$$C_{D_L} = C_{D_i} + C_{D_v} \tag{10}$$

Induced drag (C_{D_i}):

$$C_{D_i} = \frac{C_L^2}{\pi A e^*} \tag{11}$$

Where e* is the induced span efficiency factor.

The total drag due to lift is given as:

$$C_{D_L} = \frac{C_L^2}{\pi A e^*} + C_{D_v} \tag{12}$$

Since the viscous drag changes directly with C_L^2, The total drag due to lift is often expressed as:

$$C_{D_L} = \frac{C_L^2}{\pi A e} \tag{13}$$

where *e* is the span efficiency factor including viscosity effects:

$$e = \frac{1}{\pi A\left[\frac{1}{\pi A e^*} + \frac{\partial C_{D_v}}{\partial C_L^2}\right]} \tag{14}$$

2.2.2 Body Aerodynamics

Lift Prediction: The normal force curve slope, $C_{N\alpha}$, for bodies of revolution (ogival or conical noses with cylindrical afterbodies) is estimated using empirical charts based on maximum frontal area. For non-standard nose shapes, experimental data is recommended [12].

For non-linear angles of attack, the lift coefficient, based on body base area (S_b), is predicted using cross-flow analysis [16]:

$$C_L = 2\,\alpha + c_{d_c} \frac{S_P}{S_b}\,\alpha^2 \tag{15}$$

where α is the angle of attack (radians), S_p is the body planform area, S_b is the body base area, and C_{dc} is the cross-flow drag coefficient obtained from established references.

Drag Prediction: Using slender body theory, the zero-lift drag coefficient, based on frontal area, is given by:

$$C_{D_0} = C_f\,\frac{S_S}{S_B} + C_{D_{N2}} + C_{D_A} + C_{D_{(NC)}} + C_{D_{N1}} + C_{D_b} \tag{16}$$

Where;

- C_f is the turbulent flat-plate skin friction coefficient,
- $\frac{S_S}{S_B}$ is the wetted to frontal area ratio,
- $C_{D_{N2}}$ and C_{D_A} are wave drag coefficients based on maximum frontal area,
- $C_{D_{N1}}$ is the wave drag coefficient of spherically blunted noses,
- $C_{D_{(NC)}}$ is the interference drag coefficient acting on the afterbody due to center body (cylindrical section) and the nose
- C_{D_b} is the base drag coefficient, defined as:

$$C_{D_b} = -C_{P_b}\left(\frac{d_b}{d}\right)^2 \tag{17}$$

where $-C_{P_b}$ is the base pressure coefficient and d_b/d is the ratio of the base diameter to the maximum body diameter.

The total drag at angle of attack is the sum of the zero-lift drag and the drag increment due to angle of attack:

$$C_D = C_{D_0} + C_D(\alpha) \tag{18}$$

For supersonic flow, the drag increment, based on body base area, is determined as:

$$C_D(\alpha) = 2\,\alpha^2 + c_{d_c}\frac{S_P}{S_b}\,\alpha^3 \tag{19}$$

where S_p is the planform area, S_b is the base area, and α is the angle of attack in radians.

2.2.3 Wing-Body Aerodynamics

Wing-body lift accounts for interference effects using empirical factors derived from DATCOM:

a) Panel fixed at zero incidence to the body and the angle of attack of combination varied, the lift is given by the following equation

$$(C_{L_\alpha})_{WB} = \left[K_N + K_{W(B)} + K_{B(W)}\right] + (C_{L_\alpha})_e\,\frac{S_e}{S_w} \tag{20}$$

b) Body kept at zero angle of attack and wing incidence varied, the lift is given by the following equation

$$(C_{L_\alpha})_{WB} = \left[k_{W(B)} + k_{B(W)}\right] + (C_{L_\alpha})_e\,\frac{S_e}{S_w} \tag{21}$$

Where;

- $K_{W(B)}$ and $K_{B(W)}$ are interference factors derived from Ref. [12] dependent on the platform type and body/wing geometry [12].
- $k_{W(B)}$ and $k_{B(W)}$ are obtained from Ref. [12].

For all speed regimes, the lift is given by:

$$C_N = \left[K_N + K_{W(B)} + K_{B(W)}\right] + (C_{L_\alpha})_e\,\alpha\,\frac{S_e}{S_w} + I_{vB(W)}\left(\frac{\Gamma}{2\pi\alpha V r}\right)\frac{r}{b_w}\,\frac{S_w}{S_B}\,\frac{q}{q_\infty}\,\alpha (C_{L_\alpha})_w \tag{22}$$

Where; $I_{vB(W)}$ is the interference factor for a lifting surface mounted on the body centerline, $\left(\frac{\Gamma}{2\pi\alpha V r}\right)$ is the nondimensional vortex strength [17], $\frac{r}{b_w}$ is the ratio of the radius of the body at the midpoint of the exposed root chord of the lifting panel to the span of the panel, $\frac{S_w}{S_B}$ is the ratio of projected panel area to the body frontal area, $\frac{q}{q_\infty}$ is the dynamic pressure ratio acting on the panel. This value can either be assumed to be unity when the calculation is at zero height.

The zero-lift drag is the sum of individual component contributions:

$$(C_{D_0})_{WB} = (C_{D_0})_W + (C_{D_0})_B\,\frac{S_B}{S_{ref}} \tag{23}$$

Where $(C_{D_0})_W$ and $(C_{D_0})_B$ are the wing and body zero-lift drag coefficients.

Total drag is defined as:

$$(C_D)_{WB} = (C_{D_0})_{WB} + (C_{D_L})_{WB} \tag{24}$$

The drag due to lift is:

$$(C_{D_L})_{WB} = (C_{D_L})_W + [C_D(\alpha)]_B\,\frac{(S_B)_{ref}}{S_w} \tag{25}$$

Where $(C_{D_L})_W$ is the wing's drag due to lift and $[C_D(\alpha)]_B$ is the body's angle of attack drag based on its maximum frontal area.

2.3 Genetic Algorithm Optimization Framework

The numerical optimization method employed is based on the Genetic Algorithm (GA), a global optimization technique founded on natural selection and evolutionary behavior [18]. Unlike traditional optimization methods that start with a single guess and follow a deterministic path to the nearest local optimum, a GA tests many solutions simultaneously. It builds the next set of solutions using chance-based rules, allowing GA to work effectively with irregular, discontinuous, or noisy functions such as aerodynamic performance [1].

The procedure follows an iterative cycle of evaluation, selection, reproduction, and replacement [18]:

1. **Encoding**: Design variables are represented as chromosomes (real-valued encoding for continuous parameters).
2. **Initialization**: Random population of candidate designs generated within specified ranges
3. **Fitness Evaluation**: Each individual is evaluated using MAPP (fitness = L/D ratio)
4. **Selection**: Tournament selection (randomly select k individuals, choose the best)
5. **Genetic Operators**: Uniform crossover and mutation.
6. **Replacement**: Elitist strategy (best individuals preserved)

The GA optimization shell is integrated with MAPP through a FORTRAN subroutine as:

1. GA provides design variable values (wing dimensions, body dimensions, wing position)
2. MAPP constructs geometry and calculates C_L and C_D at specified conditions
3. GA computes fitness = C_L/C_D
4. GA applies genetic operators to generate a new population

GA Parameters:

- Population Size: 100 individuals
- Maximum Generations: 200
- Crossover Probability: 0.5
- Mutation Probability: 0.04
- Crossover Type: Uniform crossover

3. Validation Methodology

Before utilizing MAPP for optimization, a validation study was conducted comparing its results with previously published experimental data [19] at Mach 1.99 and Reynolds number 6.0 million (based on body length). Experimental data from scientific papers presented in chart form were converted into numerical data using the "DigitizeIt" program. The validation compared longitudinal aerodynamic characteristics for wing-alone, body-alone, and wing-body configurations.

Validation Configuration:

Body: Ogive nose with cylindrical body, total length 10.5, nose length 3.1875, diameter 1.125 Wing: Aspect ratio 4.0, leading edge angle 45°, taper ratio 0.0, double wedge airfoil, thickness-to chord ratio 8%, maximum thickness at 50% chord

Lift Coefficient Comparison: MAPP demonstrated excellent agreement with experimental results across all three configurations, as given in Table 2. Average errors were -4.12%, -2.85%, and +1.41% for wing alone, body alone, and wing-body configurations, respectively, all within acceptable engineering accuracy for preliminary design.

Drag Coefficient Comparison: Wing-alone and wing-body drag predictions showed good agreement, with average errors of -3% and +5.6%, respectively. The body-alone drag exhibited a significant discrepancy with an average error of +40.1% at low angles of attack, attributed to differences in base drag modeling between MAPP and experimental methods as given in Table 3.

The MAPP provides reliable predictions for lift across all configurations, with average errors generally within ±5%. Drag coefficient predictions are reliable for wing-alone and wing-body configurations, while body-alone drag requires careful interpretation due to base drag modeling differences.

Table 2. Comparison of lift coefficient predictions from MAPP with experimental results at Mach = 1.99

[deg]	**Wing**			**Body**			**Wing-Body**		
α	**C_L MAPP**	**C_L Exp.**	**Error %**	**C_L MAPP**	**C_L Exp.**	**Error %**	**C_L MAPP**	**C_L Exp.**	**Error %**
0.0	0.000	0.000	0.000	0.000	0.000	0.000	0.000	0.000	0.000
1.0	0.199	0.215	-8.023	0.039	0.040	-3.216	0.309	0.320	-3.577
2.0	0.398	0.420	-5.478	0.085	0.090	-5.626	0.626	0.670	-7.071
3.0	0.601	0.656	-9.095	0.139	0.141	-1.178	0.956	0.990	-3.597
4.0	0.811	0.864	-6.591	0.201	0.210	-4.368	1.302	1.320	-1.420
5.0	1.029	1.130	-9.865	0.271	0.274	-1.196	1.667	1.720	-3.185
6.0	1.254	1.310	-4.433	0.348	0.356	-2.295	2.051	2.100	-2.368
7.0	1.469	1.520	-3.498	0.433	0.466	-7.631	2.427	2.440	-0.526
8.0	1.682	1.730	-2.836	0.527	0.521	1.189	2.812	2.760	1.835
9.0	1.895	1.940	-2.402	0.631	0.630	0.163	3.203	3.110	2.917
10.0	2.104	2.120	-0.738	0.745	0.740	0.626	3.602	3.460	3.944
11.0	2.311	2.320	-0.373	0.870	0.877	-0.775	4.009	3.750	6.449
12.0	2.514	2.500	0.575	1.009	1.010	-0.075	4.423	4.200	5.044
13.0	2.714	2.650	2.345	1.164	1.210	-3.942	4.848	4.550	6.151
14.0	2.909	2.830	2.722	1.333	1.370	-2.801	5.282	5.100	3.447
15.0	3.099	3.040	1.913	1.520	1.530	-0.632	5.728	5.400	5.721
Average error			-4,12			-2.85			1,41

Table 3. Comparison of drag coefficient predicted from MAPP with experimental results at Mach = 1.99

[deg]	**Wing**			**Body**			**Wing-Body**		
α	C_D MAPP	C_D Exp.	Error %	C_D MAPP	C_D Exp.	Error %	C_D MAPP	C_D Exp.	Error %
0	0.094	0.090	4.26	0.3500	0.170	51.43	0.443	0.41	6.77
1	0.097	0.098	-1.00	0.3507	0.174	50.38	0.447	0.43	4.47
2	0.107	0.105	1.95	0.3530	0.175	50.42	0.460	0.45	2.17
3	0.124	0.136	-9.44	0.3573	0.176	50.74	0.482	0.5	-3.11
4	0.149	0.164	-9.87	0.3640	0.177	51.38	0.513	0.54	-5.07
5	0.183	0.195	-6.46	0.3736	0.192	48.61	0.557	0.61	-9.52
6	0.227	0.230	-1.42	0.3864	0.208	46.18	0.613	0.67	-8.65
7	0.276	0.290	-5.02	0.4029	0.223	44.65	0.680	0.75	-10.44
8	0.333	0.348	-4.48	0.4236	0.238	43.82	0.757	0.84	-10.44
9	0.397	0.406	-2.19	0.4491	0.268	40.33	0.847	0.93	-10.39
10	0.468	0.479	-2.28	0.4800	0.298	37.91	0.950	1.06	-11.58
11	0.546	0.581	-6.49	0.5171	0.342	33.86	1.060	1.20	-13.21
12	0.629	0.640	-1.83	0.5614	0.386	31.24	1.200	1.32	-10.00
13	0.717	0.742	-3.55	0.6141	0.445	27.54	1.330	1.50	-12.78
14	0.81	0.815	-0.67	0.6756	0.504	25.40	1.480	1.64	-10.81
15	0.906	0.917	-1.19	0.7480	0.591	20.99	1.650	1.84	-11.52
Average error			-3			40.12			5.6

4. Results and Discussion

4.1 Wing-Alone Optimization

Three wing optimization cases were performed at different Mach numbers (1.5, 3.5, and 4.0). The Non-dimensional design variables with respect to MAC included tip chord, root chord, and semi-span.

Case 1: Wing at Mach 1.5,

Flow Conditions:

- Mach Number: 1.5
- Reynolds Number: 5.5×10^6 (based on MAC)
- Angle of Attack: 3.0°
- Airfoil: Double wedge
- Thickness-to-chord ratio: 8%
- Maximum thickness location: 50% chord
- Leading edge: Sharp

Design Variable Ranges:

Tip chord range	0 (fixed)
Root chord range	3.74 – 7.43
Semi-span range	1.25 – 3.74

Optimization Results:

Table 4. Initial and final aerodynamic coefficients for case 1.

Item	C_L	ΔC_L%	C_D	ΔC_D%	C_L/C_D	$\Delta C_L/C_D$%
Initial Configuration	0.1342		0.023365		5.7436	
Final Configuration	0.11832	-11.83	0.01881	-19.49	6.289	9.495

Discussion: The improved configuration achieved a 9.5% improvement in lift-to-drag ratio despite a reduction in lift coefficient, primarily due to a 19.5% reduction in drag.

The initial and final configurations are shown in Figure 1.

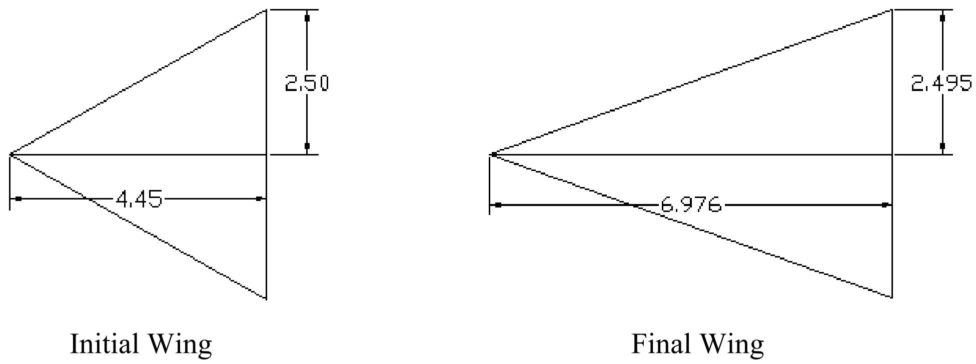

Figure 1. Initial and final wing configuration at Mach=1.5 and $\alpha=3.0^0$

Case 2: Wing Optimization at Mach 3.5

Flow Conditions:

- Mach Number: 3.5

- Reynolds Number: 10×10^6 (based on MAC)
- Angle of Attack: 3.5°
- Airfoil: Biconvex
- Thickness-to-chord ratio: 6%
- Maximum thickness location: 50% chord
- Leading edge: Sharp

Design Variable Ranges:

Tip chord range	0.25 – 1.25
Root chord range	1.25 – 2.25
Semi-span range	1.25 – 2.25

Optimization Results:

Table 5. Initial and final aerodynamic coefficients for case 2.

Item	C_L	ΔC_L%	C_D	ΔC_D%	C_L/C_D	$\Delta C_L/C_D$%
Initial Configuration	0.0793		0.0126		6.293	
Final Configuration	0.083421	5.196	0.011501	-8.72	7.253	15.255

Discussion: The improved configuration achieved a 15.3% improvement in lift-to-drag ratio, with simultaneous lift increase (5.2%) and drag reduction (8.7%)..

Figure 2 illustrates the initial and final wing geometry

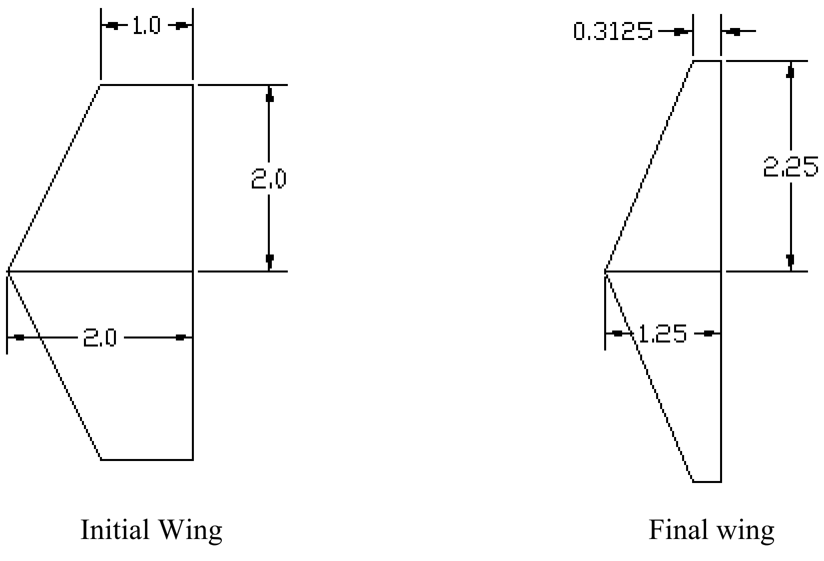

Figure 2. Initial and final wing configuration at Mach=3.5 and α=3.5^0

Case 3: Wing Optimization at Mach 4.0

Flow Conditions:

- Mach Number: 4.0
- Reynolds Number: 12×10^6 (based on MAC)
- Angle of Attack: 10°

- Airfoil: Double wedge
- Thickness-to-chord ratio: 20%
- Maximum thickness location: 50% chord
- Leading edge: Sharp

Design Variable Ranges:

Tip chord range	3.45 – 5.15
Root chord range	10.2 – 14.85
Semi-span range	8.15 – 13.75

Optimization Results:

Table 6. Initial and final aerodynamic coefficients for case 3.

Item	C_L	$\Delta C_L\%$	C_D	$\Delta C_D\%$	C_L/C_D	$\Delta C_L/C_D\%$
Initial Configuration	0.20465		0.11593		1.765	
Final Configuration	0.210363	2.791	0.098367	-15.15	2.1385	21.16

Discussion: The improved configuration achieved a substantial 21.2% improvement in lift-to-drag ratio, primarily driven by a 15.2% drag reduction.

The initial and final configuration are shown in Figure 3.

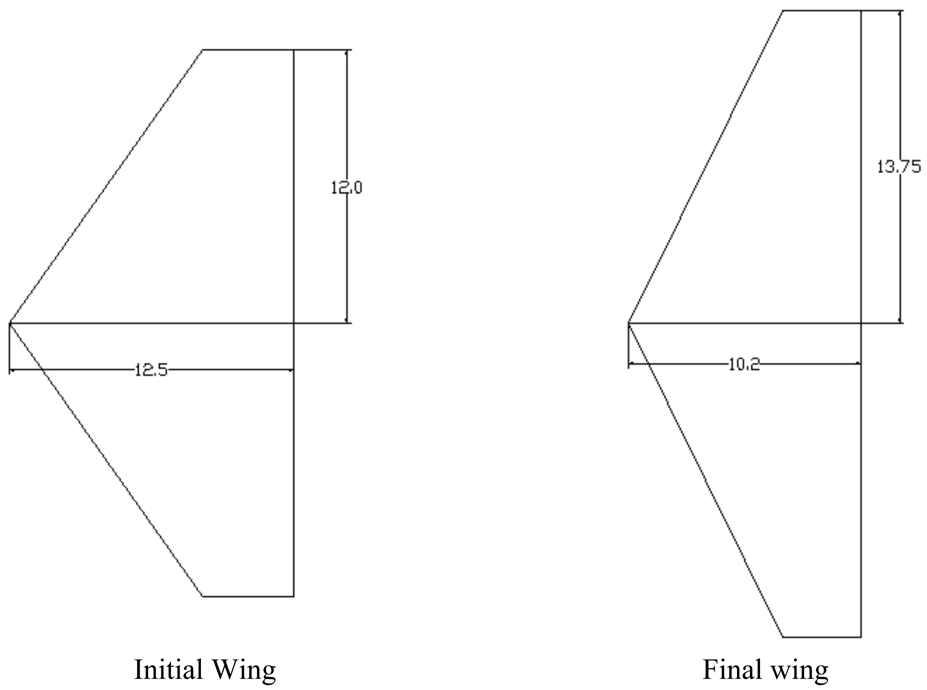

Figure 3. Final wing configuration at Mach=4.0 and α=10.0^0

4.2 Body-Alone Optimization

Three body optimization cases were performed at different Mach numbers (1.4, 2.1, and 3.95). The design variables included body length, diameter, and nose length.

Case 4: Body at Mach 1.4,

Flow Conditions and Body Parameters:

- Mach number 1.4
- Reynolds number: 5×10^6 ,

- Angle of attack: 3.9°,
- Nose type: Ogive
- Body cross-section: Circular cylinder

Design Variable Ranges:

- Body Length: 5.5 – 11.5
- Diameter: 0.5 – 1.5
- Nose Length: 2.0 – 4.0

Optimization Results:

Table 7. Initial and final aerodynamic coefficients for case 4.

Metric	Initial	Final	Change
C_L	0.19097	0.28676	+50.16%
C_D	0.35704	0.34484	-3.42%
C_L/C_D	0.534	0.832	+55.72%

Discussion: A dramatic 55.7% improvement in lift-to-drag ratio was achieved, largely due to a 50.2% increase in lift coefficient with a modest 3.4% drag reduction.

Figure 4 illustrates the (a) initial body geometry and (b) final body geometry

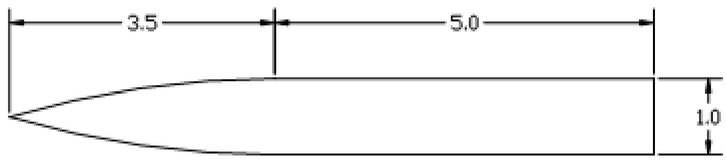

(a) Initial body configuration

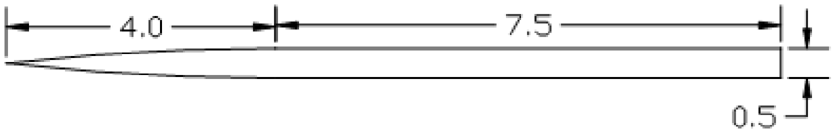

(b) Final body configuration

Figure 4. shows (a) initial body configuration (b) final body configuration at Mach=1.4 and $\alpha=3.9^0$

Case 5: : Body at Mach 2.1

Flow Conditions and Body Parameters:

- Mach number 2.1,
- Reynolds number: 9.3×10^6,
- Angle of attack: 4.7°,
- Nose type: Cone
- Body cross-section: Circular cylinder

Design Variable Ranges:

- Body Length: 10.0 – 14.35
- Diameter: 3.15 – 4.15
- Nose Length: 3.15 – 4.35

Optimization Results:

Table 8. Initial and final aerodynamic coefficients for case 5.

Metric	Initial	Final	Change
C_L	0.19268	0.19861	+3.077%
C_D	0.312285	0.17712	-43.28%
C_L/C_D	0.617	1.12135	+81.74%

Discussion: This case demonstrates the most significant improvement (81.7%) in lift-to-drag ratio across all examples, achieved through a remarkable 43.3% drag reduction.

Figure 5 illustrates the (a) initial body geometry and (b) final body geometry.

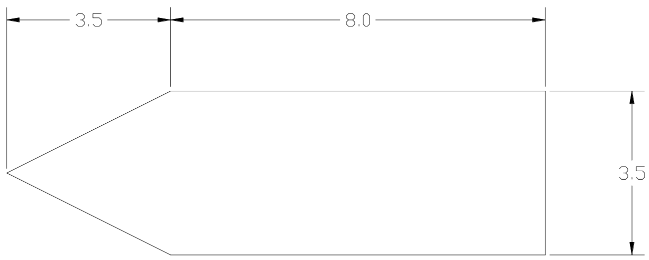

(a) Initial body configuration

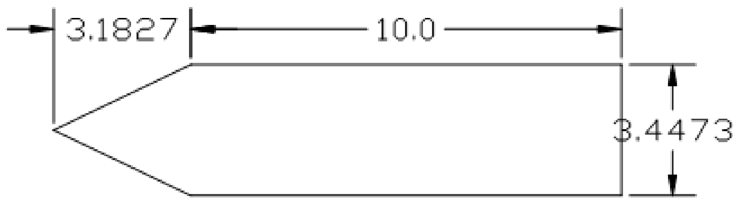

(b) Final body configuration

Figure 5. Shows (a) initial body configuration (b) final body configuration at Mach=2.1 and $\alpha=4.7^0$

Case 6: : Body at Mach 3.95

Flow Conditions and Body Parameters:

- Mach number 3.95,
- Reynolds number: 10.2×10^6,
- Angle of attack: 6.2 °,
- Nose type: Ogive
- Body cross-section: Circular cylinder

Design Variable Ranges:

- Body Length: 58.4 – 71.0
- Diameter: 16.2 – 16.8
- Nose Length: 16.0 – 18.4

Optimization Results:

Table 9. Initial and final aerodynamic coefficients for case 6.

Metric	Initial	Final	Change
C_L	0.28883	0.29601	+2.485%
C_D	0.1156	0.11774	+1.8512%
C_L/C_D	2.49854	2.51416	+0.6251%

Discussion: Minimal improvement (0.63%) was observed, suggesting that the initial configuration was already near-optimal for these conditions.

Figure 6 illustrates the (a) initial body geometry and (b) final body geometry

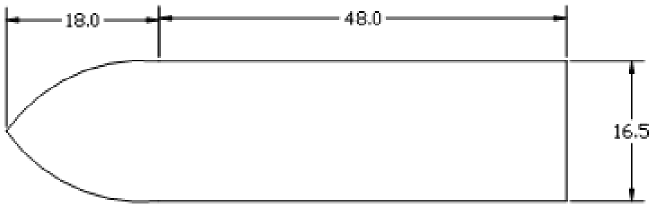

(a) Initial body configuration

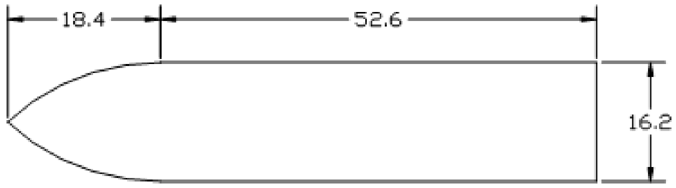

(b) Final body configuration

Figure 6. Shows (a) initial body configuration (b) final body configuration at Mach=3.95 and α=6.2^0

The body optimization showed the most dramatic improvements (up to 81.7% at Mach 2.1). Unlike wing cases, body improvements were primarily driven by substantial increases in lift coefficient (up to 50.2% at Mach 1.4) rather than drag reduction. The minimal improvement at Mach 3.95 indicates the initial configuration was already near-optimal for those conditions.

4.3 Wing-Body Optimization

Case 7: Wing-Body at Mach 1.99, Reynolds number: 6×10^6 , Angle of attack: 4.3°,

Wing-Body Description:

Parameter	Value
Airfoil section	Double wedge
Thickness-to-chord ratio	8%
Maximum thickness location	50% chord
Leading edge	Sharp
Tip chord range	0.0 – 0.6
Root chord range	1.75 – 3.0
Semi-span range	8.15 – 13.75
Nose type	Ogive

Body cross-section	Circular cylinder
Body length range	8.75 – 12.45
Diameter range	0.85 – 1.3
Nose length range	2.9 – 4.1
Wing position (distance from nose to wing leading edge)	4.5 – 6.25

Improvement Results:

Table 10. Initial and final aerodynamic coefficients for case 7.

Item	C_L	ΔC_L%	C_D	ΔC_D%	C_L/C_D	$\Delta C_L/C_D$%
Initial Configuration	0.19018		0.56483		0.336706	
Final Configuration	0.19859	4.422	0.43969	-22.15	0.45167	34.14

Discussion: The improved wing-body configuration achieved a 34.1% improvement in lift-to-drag ratio, driven primarily by a 22.2% drag reduction with a modest 4.4% lift increase.

Figures 7 and 8 illustrate the initial and final wing-body configurations, respectively.

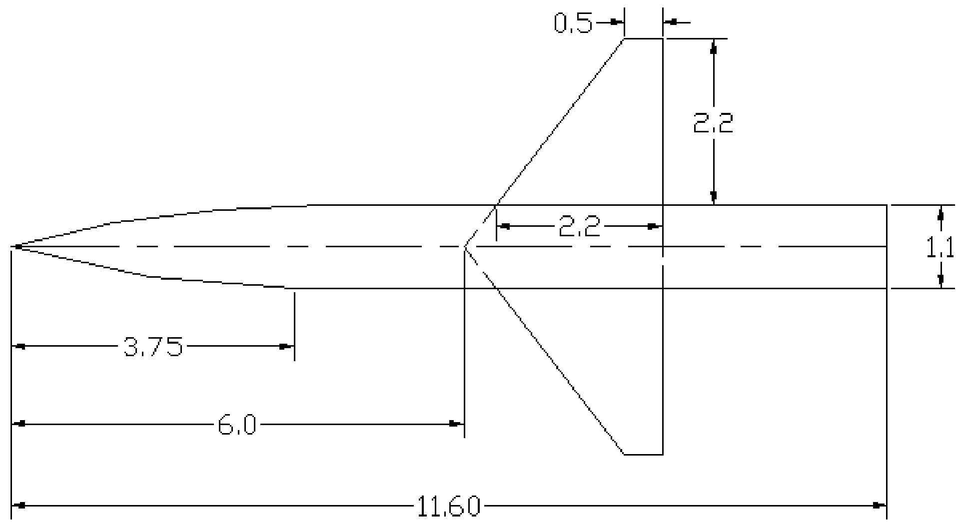

Figure 7. Initial wing-body configuration at Mach=1.99 and α=4.3^0

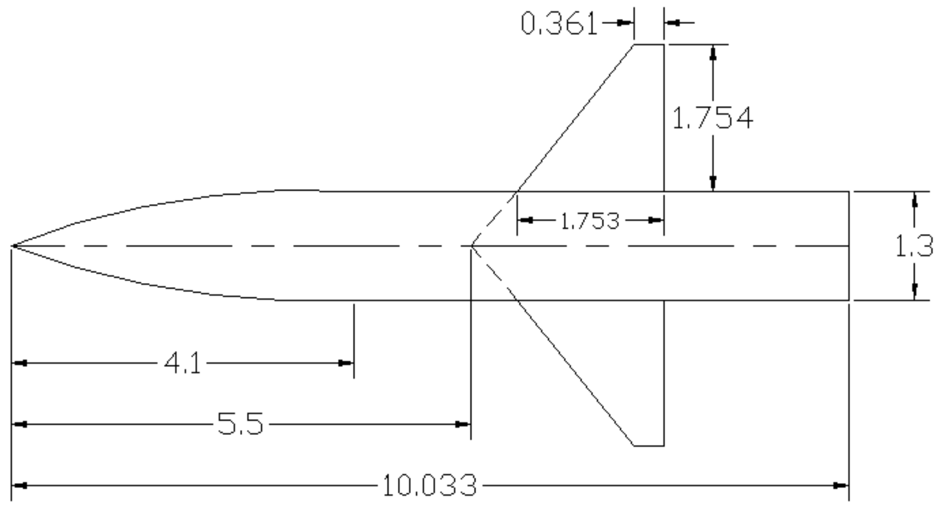

Figure 8. Final body configuration at Mach=1.99 and α=4.3^0

4.4 Discussion

The optimization results demonstrate that the genetic algorithm based approach successfully improves aerodynamic efficiency across all configurations [9-11, 20, 21]. Key observations include:

1. **Configuration-Specific Behavior:** Wings benefit primarily from drag reduction (8.7-19.5%), bodies from lift increase (up to 50.2%), and wing-body combinations from a balance of both mechanisms.
2. **Mach Number Effects:** Higher Mach numbers yielded greater improvements for wings (9.5% at Mach 1.5 to 21.2% at Mach 4.0), while body improvements were most dramatic at lower supersonic Mach numbers (81.7% at Mach 2.1).
3. **Design Variable Selection:** The chosen design variables (root chord, tip chord, span for wings; length, diameter, nose length for bodies; wing position for combinations) adequately captured essential geometric features affecting aerodynamic performance.
4. **Tool Integration Success:** The GA-MAPP integration through FORTRAN subroutine successfully automated aerodynamic design optimization, significantly reducing the need for manual iteration or exhaustive wind tunnel testing.

5. Conclusions

This study successfully developed and demonstrated a numerical optimization framework integrating a Genetic Algorithm with the MAPP for improved aerodynamic design of wing-body configurations at supersonic speeds. The following conclusions are drawn:

1. **Validation of MAPP:** MAPP demonstrated excellent agreement with experimental results for lift coefficients across all configurations (average errors within ±5%). Drag predictions were reliable for wing-alone and wing-body configurations, with body-alone drag requiring careful interpretation due to base drag modeling differences.
2. **Wing Optimization:** GA successfully improved L/D for all wing cases (9.5-21.2%), with higher Mach numbers yielding greater benefits. Drag reduction (8.7-19.5%) was the primary driver of improvement.
3. **Body Optimization:** Body configurations showed the most dramatic improvements (up to 81.7% at Mach 2.1), primarily driven by substantial lift increases (up to 50.2%). Near-optimal initial designs showed minimal improvement, demonstrating the importance of baseline selection.
4. **Wing-Body Optimization:** Integrated optimization achieved 34.1% L/D improvement through combined lift increase (4.4%) and drag reduction (22.2%). Including wing position as a design variable proved valuable for improved aerodynamic integration.
5. **GA Effectiveness:** The genetic algorithm proved robust and effective for mono-objective aerodynamic optimization problems involving non-linear and discontinuous design spaces characteristic of supersonic flows.

6. Acknowledgment

The authors would like to express their sincere gratitude to the Aeronautical Engineering Department, Faculty of Engineering, University of Zawia for providing the support necessary to complete this research.

REFERENCES

[1] Goldberg, D. E., Deb, K., and Clark, J. H., "Genetic Algorithms, Noise, and the SIZING of Populations," in: Complex System. Vol. 6, Complex System Pub., Inc., 1992, pp. 333-362.

[2] Anderson, J. D., Jr. *Fundamentals of Aerodynamics*. 5th ed., McGraw-Hill, 2011.

[3] Anderson, M. B., Burkhalter, J. E., and Jenkins, R. M. "Missile Aerodynamic Shape Optimization Using Genetic Algorithms," *Journal of Spacecraft and Rockets*, Vol. 37, No. 5, 2000, pp. 663-669.

[4] Omer, Elhassen Ali Ahmed, Hana Moftah Momen, and Rayan Nassr Yahia. 'Enhancement of Airfoil Aerodynamic Characteristics by Surface Modifications'. *University of Zawia Journal of Engineering Sciences and Technology* 1, no. 1 (2024): 60–71. https://doi.org/10.26629/uzjest.2023.06.

[5] Omer, Elhassen, Ali Alkharboushi, and Zainab Ahmed. 'Numerical Study of Turbulent Flow Aerodynamics Around a Multi-Element Airfoil'. University of Zawia Journal of Engineering Sciences and Technology 3, no. 1 (2025): 26–42. https://doi.org/10.26629/uzjest.2025.03.

[6] Jolgam, Shaban A., Ahmed R. Ballil, Andrzej F. Nowakowski, and Abdulmaged K. Shati. 'Numerical Simulations of Compressible Two-Component Flows with General Equation of State'. University of Zawia Journal of Engineering Sciences and Technology 2, no. 1 (2024): 61–80. https://doi.org/10.26629/uzjest.2024.07.

[7] Elfaghi, Abdulhafid, Ashraf Ali Omar, and Waqar Asrar. 'Higher-Order Compact-Flow Field-Dependent Variation (HOC-FDV) Method for Solving Two-Dimensional Navier-Stokes Equations'. International Journal for Computational Methods in Engineering Science and Mechanics 16, no. 4 (2015): 256–63. https://doi.org/10.1080/15502287.2015.1048386.

[8] Sasaki, D., Obayashi, S., and Nakahashi, K. "Wing-Body Configuration Optimization for Supersonic Transport Using Multiobjective Evolutionary Algorithm," *Journal of Aircraft*, Vol. 41, No. 5, 2004, pp. 1134-1142.

[9] Oyama, A., Obayashi, S., and Nakahashi, K. "Euler/Navier-Stokes Optimization of Supersonic Wing Design Based on Evolutionary Algorithm," *AIAA Journal*, Vol. 37, No. 10, 1999, pp. 1327-1328.

[10] Liu, J.-L. and Chen, J.-L. "Intelligent Genetic Algorithm with a Gradient-Based Local Search Applied to Supersonic Wing Planform Optimization," *Journal of Mechanics*, Vol. 23, No. 4, 2007, pp. 285-294.

[11] Michelotti, A., Cavini, A., Giacopino, R., Misino, F., and Piottoli, L. "Implementation of genetic algorithms for supersonic airfoil optimization," *IOP Conference Series: Materials Science and Engineering*, Vol. 1226, 2022, p. 012030.

[12] McDonnell Douglas Corp.: USAF Stability and Control DATCOM. Air Force Flight Dyn., U.S Air Force, Oct. 1960. (Revised Jan. 1974).

[13] McDonnell Douglas Astronautics Company East. St Louis, Missouri: The USAF Stability and Control Digital DATCOM. AFFDL-TR-76-45, November 1976.

[14] J. E. Burkhalter and R. M. Jenkins: Design of a Guided Missile Interceptor Using a Genetic Algorithm. *Journal of Spacecraft and Rockets* Vol. 38, No. 1, January-February 2001. Auburn University, Auburn, Alabama 36830.

[15] Kaattari. G. E.: Pressure Distribution on Triangular and Rectangular Wings to High Angles of Attack-Mach Numbers 1.45 and 1.97. NACA RM A54D19, 1954.

[16] Dennis, R. W., and Cunningham, B. E.: Forces and Moments on Inclined Bodies at Mach Numbers from 3.0 to 6.0. NACA RM A54E03, 1954.

[17] Jack N. Nielsen, Elliott D. Katzen, and Kenneth K. Tang: Lift and Pitching Moment Interference between a Pointed Cylindrical Body and Triangular Wings of Various Aspect Ratios at Mach Numbers of 1.5 and 2.02. NACA RM A50F06.

[18] Michael Wetter: GenOpt® Genetic Optimization Program. Technical Report LBNL-54199, January 5, 2004.

[19] Koenig, D. G.: Low-Speed Tests of Semispan Wing Models at Angles of Attack from 0° to 180°. NASA Memo 2-27-59A.

[20] Rao, H., Shi, Y., Bai, J., Chen, Y., Yang, T., and Li, J. "Aerodynamic optimization design of supersonic wing based on discrete adjoint," *Aerospace*, Vol. 10, No. 5, 2023, p. 420.

[21] Ye, L., Ye, Z., Ye, K., Wu, J., and Miao, S. "A low-boom and low-drag design method for supersonic aircraft and its applications on airfoils," *Advances in Aerodynamics*, Vol. 3, 2021, p. 25.